Supplementary Material to: Ultrafast magnetization induced by linearly polarized pulses is widespread in nonmagnetic semiconductors

Xiangzhou Zhu,[1,*] Junfeng Qiao,[2,†] Nicola Marzari,[2,‡] and M. Calandra[1,§]

[1] *Department of Physics, University of Trento, Trento, Italy*
[2] *Theory and Simulation of Materials (THEOS), and National Centre for Computational Design and Discovery of Novel Materials (MARVEL), École Polytechnique Fédérale de Lausanne, Lausanne, Switzerland*

CONTENTS

* xiangzhou.zhu@unitn.it
† junfeng.qiao@epfl.ch
‡ nicola.marzari@epfl.ch
§ m.calandrabuonaura@unitn.it

I. ROBUST REGARDING THE PHOTOEXCITED CARRIER DENSITY

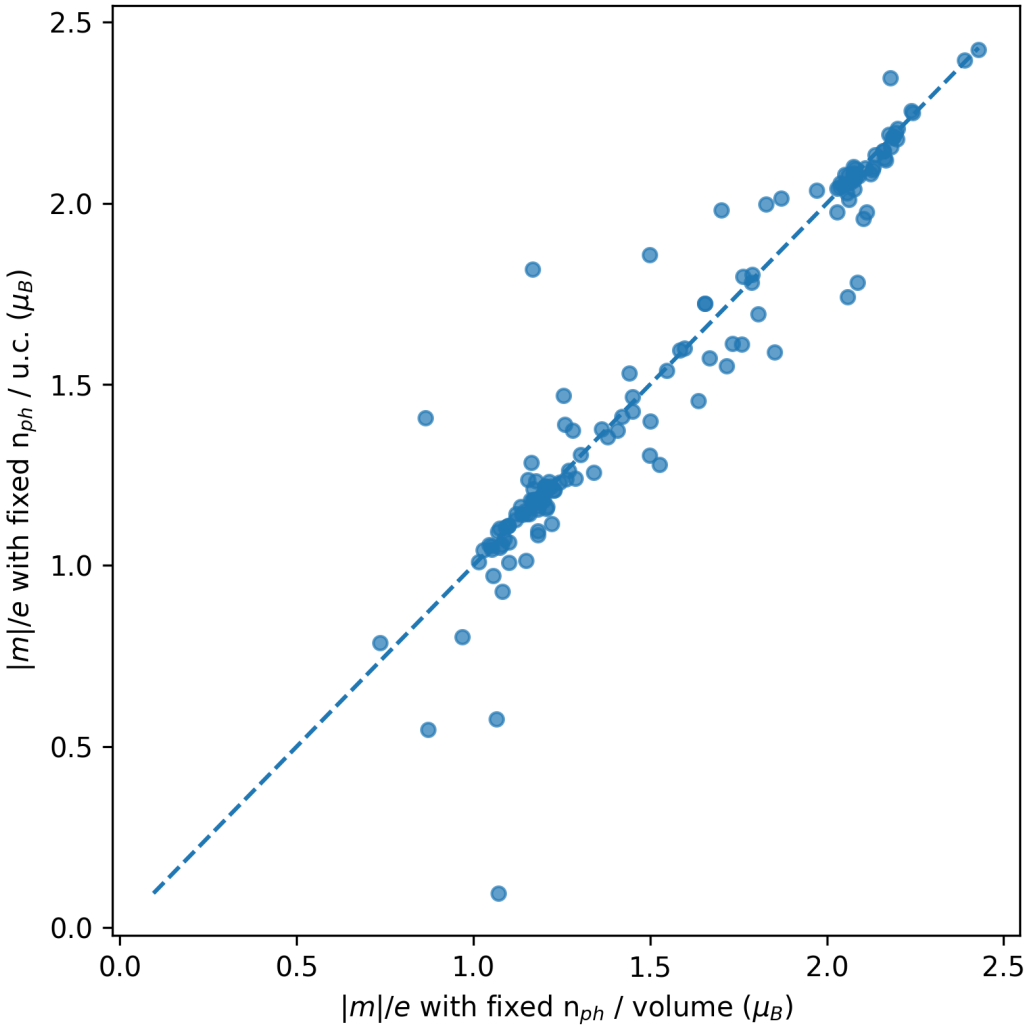

Fig. S1. Comparison of the light induced absolute magnetic moment per excited carrier, obtained using two approaches in fixing the carrier density n_{ph}**.** Each point represents one material. To avoid the possible convergence problem for too small carrier density, only densities larger than 0.15 e^-/u.c. are considered. The vertical axis represents the case fixing electron per unit cell 0.2 n_{ph}/u.c., while the horizontal axis fixing electron per volume 1.2×10^{-4} e^-/bohr^3. The dashed line indicates the exact agreement. Most systems lie close to the line with the averaged difference of 0.017 μ_B, showing that the induced magnetic moment is robust with the choice of carrier density.

II. ROLE OF STRUCTURE OPTIMIZATION

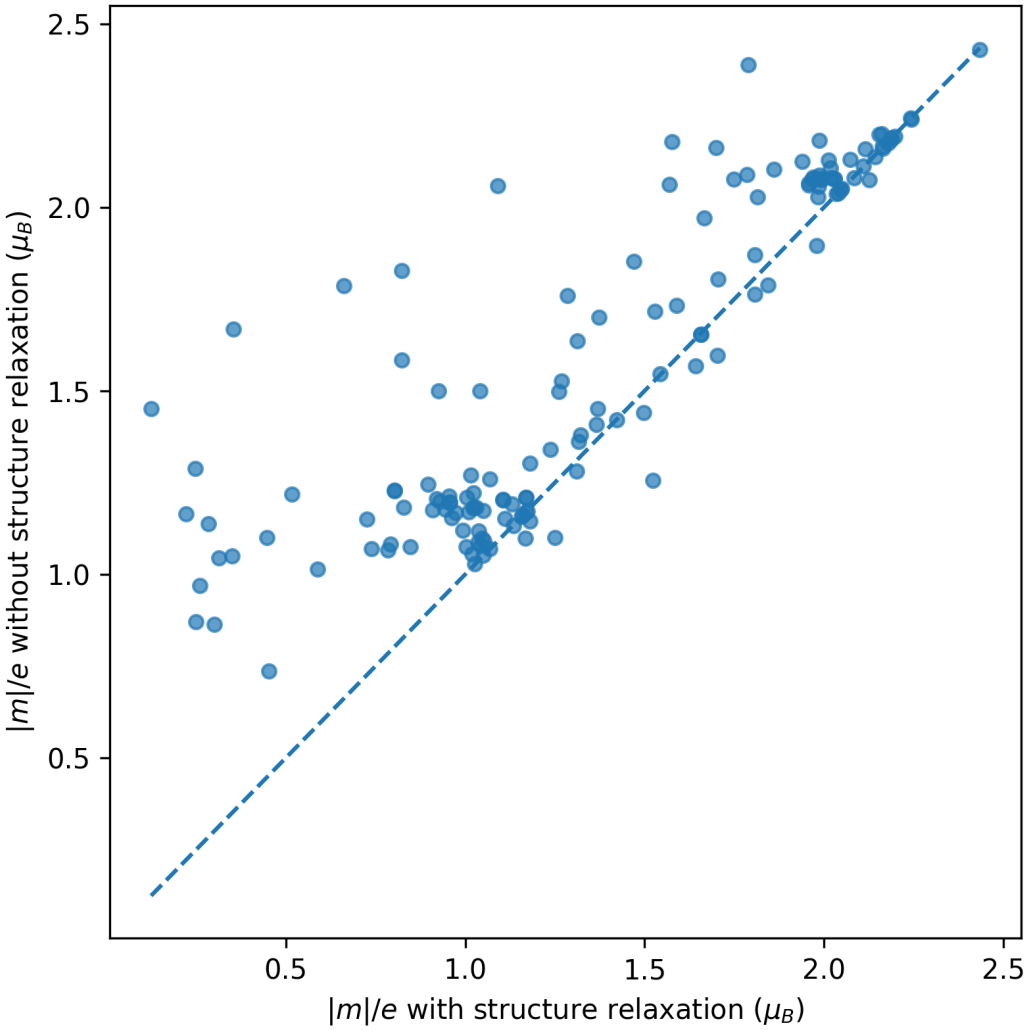

Fig. S2. Comparison of the light induced absolute magnetic moment per excited carrier, obtained with/without additional structure optimization (horizontal/vertical axis). Each point represents one material. The carrier density is fixed to 1.2 e−/bohr^3 and only electron larger than 0.15 e$^-$/u.c. is considered. The dashed line indicates the exact agreement. Points above the line indicate that the unrelaxed structure gives a larger magnetic response than the relaxed structure, suggesting that structural relaxation generally reduces induced magnetization for a subset of systems with an averaged difference of 0.21 μ_B.

III. PROMISING CANDIDATES FOR EXPERIMENTAL VERIFICATION

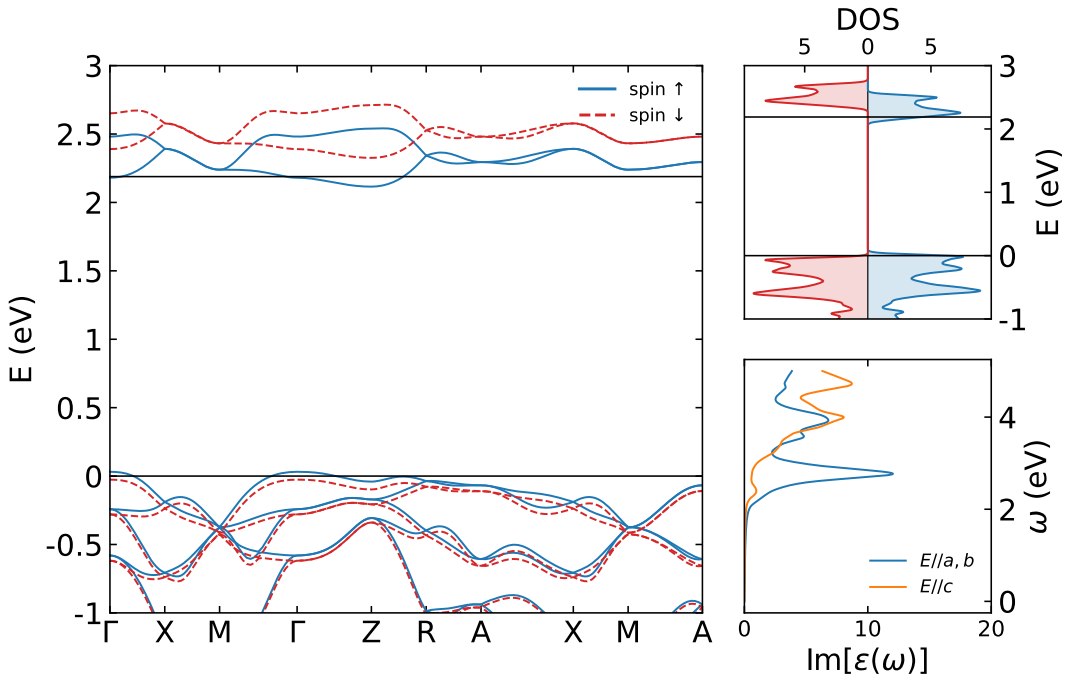

Fig. S3. Electronic and optical properties of $VOPO_4$ in the P4/n phase (mc3d-15020). The electronic band structure and density of states are calculated for a photoexcited carrier density of $n_{\mathrm{ph}} = 0.2$ per unit cell. The photoexcited state develops an antiferromagnetic spin configuration with an induced absolute magnetic moment of $m_{\mathrm{abs}} = 2.58\ \mu_B$ and zero total magnetic moment, $m_{\mathrm{tot}} = 0$. Spin-up and spin-down channels are shown in blue and red, respectively. The imaginary part of the dielectric function is calculated using norm-conserving pseudopotentials from the PseudoDojo library [1]. The Fermi level is set to zero energy.

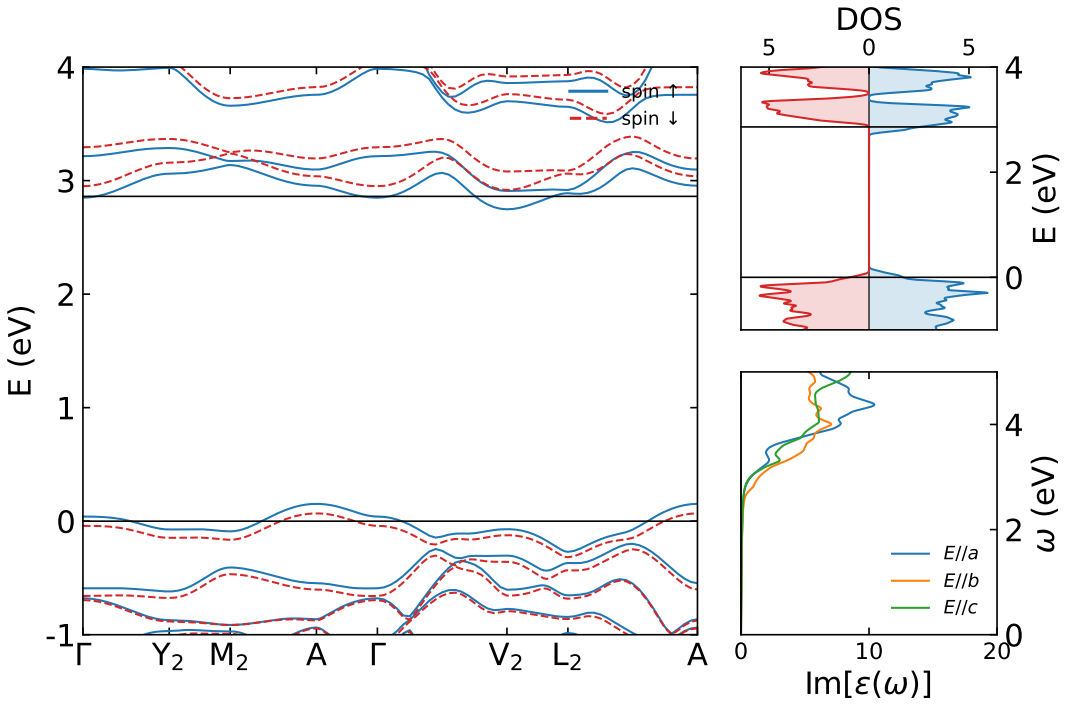

Fig. S4. Electronic and optical properties of MgV_2O_6 in the C2/m phase (mc3d-4145). The band structure and density of states are calculated for a photoexcited carrier density of $n_{\mathrm{ph}} = 0.2$ per unit cell, yielding a ferrimagnetic spin configuration with $m_{\mathrm{abs}} = 2.14\ \mu_B$ and $m_{\mathrm{tot}} = 0.31\ \mu_B$. Other computational settings and plotting conventions are the same as previous figure.

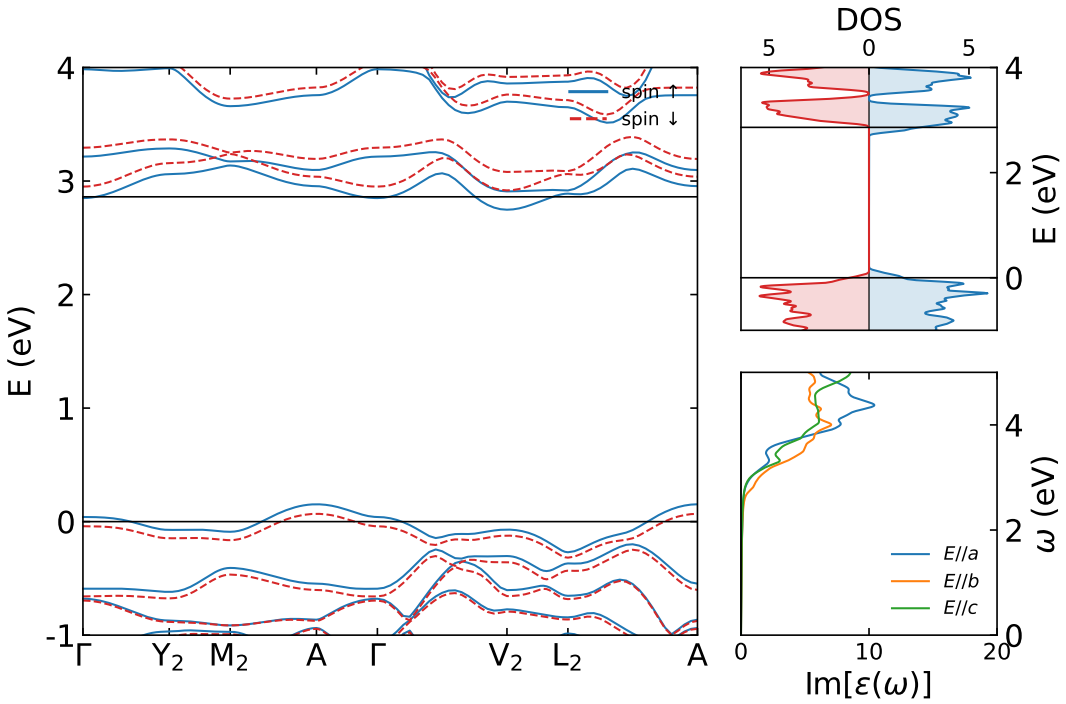

Fig. S5. Electronic and optical properties of CaV_2O_6 in the C2/m phase (mc3d-24069). The band structure and density of states are calculated for a photoexcited carrier density of $n_{\mathrm{ph}} = 0.2$ per unit cell, yielding a antiferromagnetic spin configuration with $m_{\mathrm{abs}} = 2.51\ \mu_B$ and $m_{\mathrm{tot}} = 0\ \mu_B$. Other computational settings and plotting conventions are the same as previous figure.

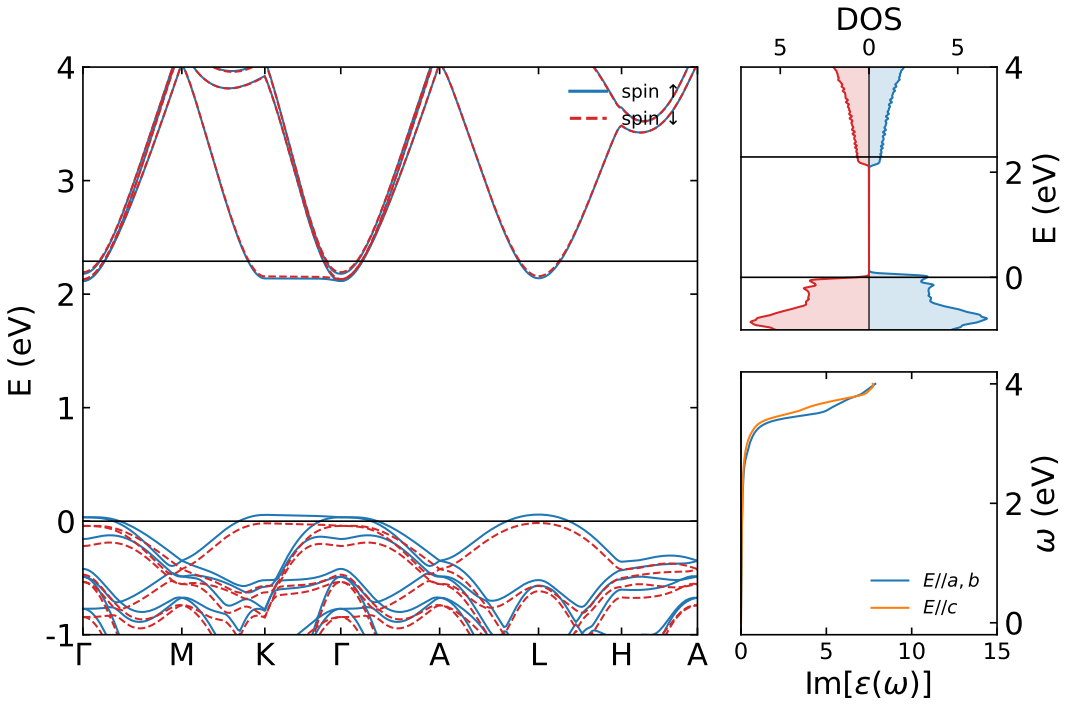

Fig. S6. Electronic and optical properties of $NaNbO_3$ in the R3c phase (mc3d-11741). The band structure and density of states are calculated for a photoexcited carrier density of $n_{\mathrm{ph}} = 0.2$ per unit cell, yielding a ferrimagnetic spin configuration with $m_{\mathrm{abs}} = 1.30\ \mu_B$ and $m_{\mathrm{tot}} = 0.96\ \mu_B$. The semilocal Kohn-Sham gap is underestimated in this calculation while an mBJ calculation gives a gap of approximately 3.3 eV [2]. Other computational settings and plotting conventions are the same as previous figure.

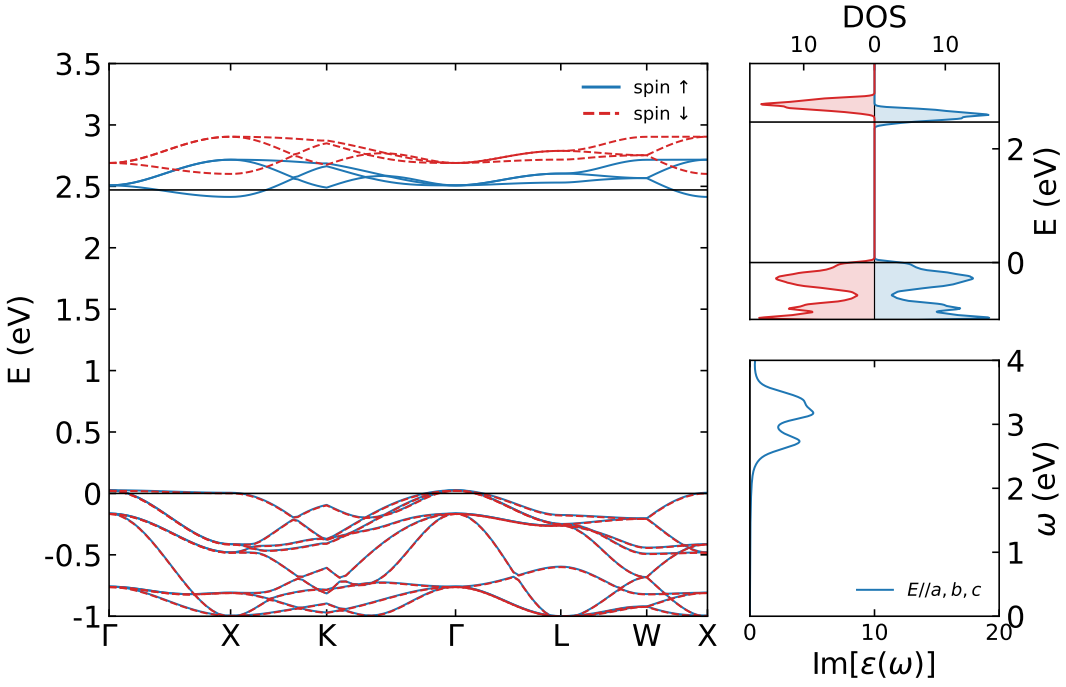

Fig. S7. Electronic and optical properties of Cs_2TiCl_6 in the $Fm\bar{3}m$ phase (mc3d-49897). The band structure and density of states are calculated for a photoexcited carrier density of $n_{\mathrm{ph}} = 0.2$ per unit cell, yielding a ferrimagnetic spin configuration with $m_{\mathrm{abs}} = 1.86\ \mu_B$ and $m_{\mathrm{tot}} = 0.33\ \mu_B$. Other computational settings and plotting conventions are the same as previous figure.

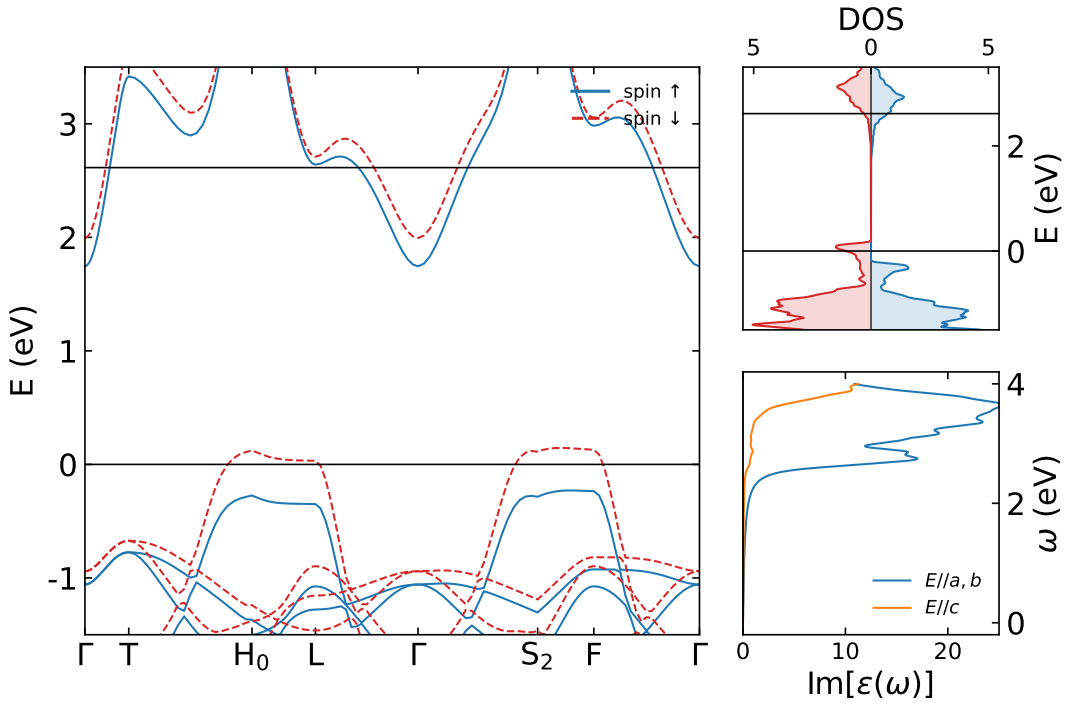

Fig. S8. Electronic and optical properties of $CuAlO_2$ in the R$\bar{3}$m phase (mc3d-76348). The band structure and density of states are calculated for a photoexcited carrier density of $n_{\mathrm{ph}} = 0.2$ per unit cell, yielding a ferromagnetic spin configuration with $m_{\mathrm{abs}} = m_{\mathrm{tot}} = 1.41\ \mu_B$. The semilocal Kohn-Sham gap is underestimated in this calculation while the reported indirect gap 2.99 eV and direct gap 3.53 eV [3]. Other computational settings and plotting conventions are the same as previous figure.

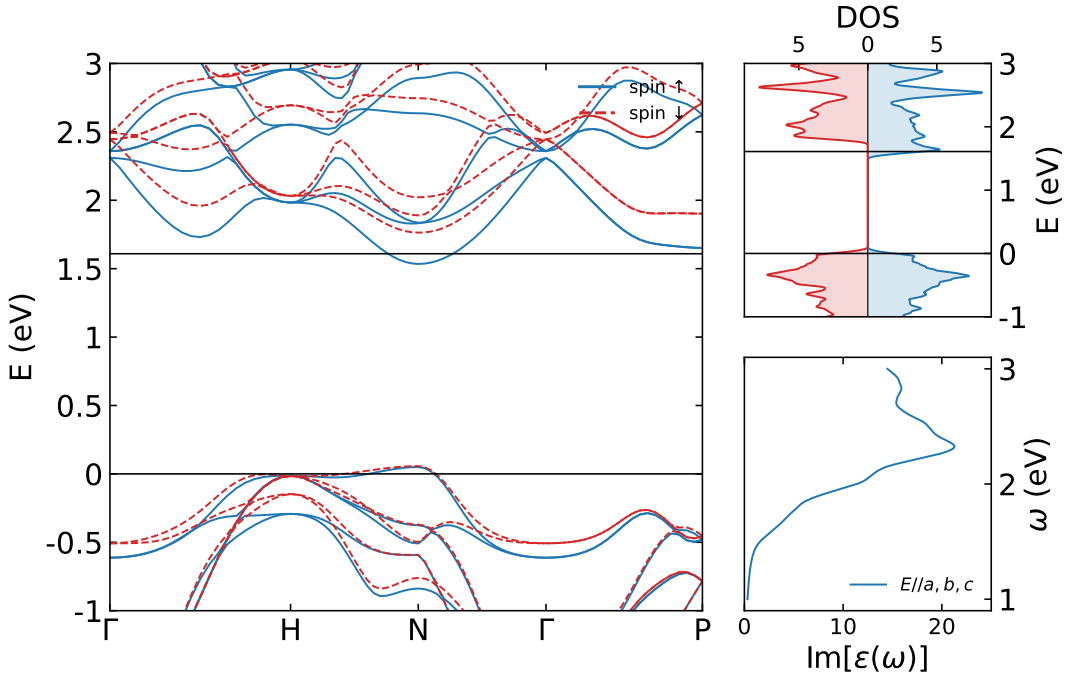

Fig. S9. Electronic and optical properties of Tl_3VSe_4 in the I$\bar{4}$3m phase (mc3d-60466). The band structure and density of states are calculated for a photoexcited carrier density of $n_{\mathrm{ph}} = 0.2$ per unit cell, yielding a ferrimagnetic spin configuration with $m_{\mathrm{abs}} = 1.60\ \mu_B$ and $m_{\mathrm{tot}} = 1.35\ \mu_B$. Other computational settings and plotting conventions are the same as previous figure.

[1] M. J. van Setten, M. Giantomassi, E. Bousquet, M. J. Verstraete, D. R. Hamann, X. Gonze, and G. M. Rignanese, The PseudoDojo: Training and grading a 85 element optimized norm-conserving pseudopotential table, Computer Physics Communications **226**, 39 (2018).
[2] K. Choudhary, Q. Zhang, A. C. E. Reid, S. Chowdhury, N. Van Nguyen, Z. Trautt, M. W. Newrock, F. Y. Congo, and F. Tavazza, Computational screening of high-performance optoelectronic materials using OptB88vdW and TB-mBJ formalisms, Sci Data **5**, 180082 (2018).
[3] J. Pellicer-Porres, A. Segura, A. S. Gilliland, A. Muñoz, P. Rodríguez-Hernández, D. Kim, M. S. Lee, and T. Y. Kim, On the band gap of CuAlO2 delafossite, Appl. Phys. Lett. **88**, 181904 (2006).